Modulating Mast Cell Activity

with Novel Siglec-8 Targeted Nanobodies

GeunAh Kim

The Graduate School
Yonsei University
Department of Medical Science

Modulating Mast Cell Activity

with Novel Siglec-8 Targeted Nanobodies

A Master's Thesis Submitted
to the Department of Medical Science
and the Graduate School of Yonsei University
in partial fulfillment of the
requirements for the degree of
Master's of Medical Science

GeunAh Kim

January 2025

This certifies that the Master's Thesis

of GeunAh Kim is approved

Thesis Supervisor Joo Young Kim

Thesis Committee Member Hyung-ju Cho

Thesis Committee Member Myeong Heon Shin

The Graduate School
Yonsei University

January 2025

ACKNOWLEDGEMENTS

First and foremost, I would like to thank my supervisor, Professor Joo Young Kim. It has been an honor to carry out my research under your dedicated support, excellent guidance, and profound expertise. Your mentorship has been invaluable to my growth as a researcher.

I would also like to extend my appreciation to my committee members, Professor Hyung-ju Cho and Professor Myeong-Heon Shin, for their constructive feedback and insightful advice on my research.

I am grateful to Dr. Donghyukc Lee for your encouragement, insightful discussions, and generous sharing of knowledge. Your support has greatly contributed to my research.

I am also deeply grateful to my lab colleagues, JinKyung, JiHyeon, ChangSin, DaHye, and RyunSeon. Working with you has been a

valuable learning experience and made my master's journey more enjoyable.

Finally, I would like to express my heartfelt thanks to my family. To my mom and dad, your support has been the foundation that allowed me to pursue my academic goals. Your support allowed me to focus on my research and complete my master's degree successfully.

To all of you, thank you.

TABLE OF CONTENTS

LIST OF FIGURES

LIST OF TABLES

ABSTRACT

Modulating Mast Cell Activity with Novel Siglec-8 Targeted Nanobodies

Mast cells play a pivotal role in allergic inflammation, making them critical targets for therapeutic intervention in conditions such as asthma and chronic urticaria. Siglec-8, an inhibitory receptor selectively expressed on mast cells and eosinophils, has been identified as a promising target due to its ability to suppress mast cell activation through ITIM-mediated signaling. In this study, we developed and characterized Siglec-8-targeted nanobodies with distinct binding properties, including homodimer and heterodimer formats.

Our results demonstrate that heterodimer nanobodies rapidly induce Siglec-8 clustering, leading to efficient suppression of mast cell activation within 1 hour of treatment. This rapid effect is followed by receptor internalization, whereas homodimer nanobodies exhibited slower but sustained inhibitory effects through prolonged receptor clustering. These findings highlight the distinct temporal and functional mechanisms of Siglec-8 nanobody variants.

This study underscores the potential of Siglec-8 clustering as a novel strategy for modulating

mast cell activity, providing a foundation for developing targeted and safer therapeutics for allergic and inflammatory disorders.

Key words : Mast cell, allergic inflammation, Siglec-8, nanobody, ITIM motif, inhibitory receptor, receptor clustering

1. INTRODUCTION

Allergic diseases, ranging from asthma to allergic rhinitis, have become increasingly prevalent in recent years, affecting millions worldwide and significantly reducing quality of life[1-4]. Conventional treatments for allergic conditions primarily target IgE-dependent pathways, with omalizumab, a widely used monoclonal antibody, serving as a prominent example[5]. Omalizumab works by binding to circulating IgE, thereby preventing it from interacting with its receptors on effector cells such as mast cells and basophils[6]. This mechanism is highly effective in managing conditions like severe asthma and chronic urticaria.

However, omalizumab and similar therapies often fail to address allergic reactions that occur via IgE-independent mechanisms. Examples of such conditions include drug allergies, insect venom allergies, and other hypersensitivity reactions[7]. As these IgE-independent allergies continue to pose significant clinical challenges, there is a critical need to develop new therapeutic approaches that can target these alternative pathways[8].

One such emerging target is Siglec-8, a receptor with potential to modulate both IgE-dependent and IgE-independent signaling in various allergic reactions[8,9]. Siglec-8 is a sialic acid-binding immunoglobulin-like lectin expressed predominantly on mast cells and eosinophils, two key cell types involved in allergic inflammation[10-12]. Importantly, Siglec-8 contains immunoreceptor tyrosine-based inhibition motifs (ITIMs) that can inhibit intracellular allergic signaling when engaged, leading to reduced activation of mast cells and eosinophils[13-17]. This inhibitory effect offers

a unique therapeutic opportunity to modulate allergic responses not only through IgE-mediated pathways but also by inhibiting MRGPRX2, a receptor that has been implicated in IgE-independent mast cell activation.

MRGPRX2 has emerged as a crucial player in mast cell activation in response to non-IgE stimuli, contributing to allergic reactions that are not addressed by conventional therapies[18-23]. The ability of Siglec-8 to inhibit MRGPRX2-mediated responses positions it as a promising therapeutic target for a broader range of allergic conditions, including those that are resistant to current treatments like omalizumab.

Building on this potential, recent clinical developments have focused on antibodies targeting Siglec-8, such as Lirentelimab, a monoclonal antibody currently under investigation[24]. Lirentelimab has demonstrated promising results in clinical trials by suppressing mast cell and eosinophil activation via Siglec-8 engagement[24]. However, Lirentelimab, like many biologics, must be administered via injection, which introduces several limitations. Additionally, as an IgG1 antibody, Lirentelimab has the potential to induce cytotoxicity in target cells, potentially leading to unintended suppression of immune responses against infections[25,26]. Recent studies have also highlighted the regulatory roles of mast cells in immune homeostasis, raising concerns that the depletion or functional inhibition of mast cells by Lirentelimab could disrupt immune system balance and contribute to unforeseen adverse effects[27,28]. Also, Injection site reactions (ISRs), such as pain, erythema, and swelling, are common side effects of subcutaneous or intravenous antibody administration. Furthermore, clinical trials have reported infusion-related reactions, which can range from mild discomfort to more serious systemic effects[29]. The parenteral administration of such therapies also means that they often take time to reach the site of allergic reactions, delaying the

onset of therapeutic effects, especially in acute allergic conditions. This delay is particularly problematic for IgE-independent allergic reactions, where immediate intervention is often necessary. Given these limitations, there is a growing interest in exploring alternative therapeutic modalities that can offer faster and more targeted treatment with fewer side effects.

Nanobodies, a class of single-domain antibody fragments derived from camelids, offer unique advantages over conventional monoclonal antibodies, including smaller size, enhanced stability, and ease of engineering[30-32]. These features facilitate precise receptor targeting, improved tissue penetration, and reduced off-target effects. In this study, we developed and characterized Siglec-8-specific nanobodies designed to induce receptor clustering, a mechanism hypothesized to enhance inhibitory signaling and suppress mast cell activation more effectively.

Our results demonstrate that heterodimer nanobodies induce rapid Siglec-8 clustering, leading to significant mast cell inhibition within a short time frame. In contrast, homodimer nanobodies exhibit slower but sustained inhibitory effects, likely due to prolonged receptor clustering at the cell surface. These findings reveal distinct temporal and functional characteristics of nanobody-induced Siglec-8 activation.

This study provides new insights into the mechanisms underlying Siglec-8 clustering and mast cell inhibition, highlighting the potential of nanobody-based therapeutics as innovative strategies for addressing allergic diseases. By overcoming the limitations of existing antibody-based treatments, these findings establish a foundation for the development of safer and more effective therapies targeting Siglec-8.

2. MATERIAL AND METHODS

2.1. Cell culture

HEK-293T cell line was purchased from the Korea Cell Line Bank. Cells were cultured in DMEM high glucose media supplemented with 10% FBS and 1% penicillin/streptomycin at 37℃ and 5% CO_2. For cell cultures, DMEM culture medium (Dulbecco's modified Eagle medium, 119995-065), Fetal bovine serum (FBS) (26140-079), Penicillin-streptomycin (15149-122, Gibco, Life technologies™, Carlsbad, CA, USA); Trypsin-EDTA 0.05% solution (25300-062, Gibco, Life technologies™, Carlsbad, CA, USA) were used.

LAD2 cell line was purchased from Applied Biological Materials. Those cells were cultured in StemPro-34 SFM (Thermo Fisher Scientific, MA, USA) with StemPro-34 nutrient supplement (2.5%, Thermo Fisher Scientific, MA, USA) with L-glutamine (2 mM, Gibco, CA USA), penicillin/streptomycin (1%, Gibco, CA, USA), and recombinant human SCF (100 ng/ml, R&D systems, MN, USA). Half of the medium was replaced weekly by adding an equal volume of fresh medium containing SCF. The cell density was maintained at 2-5×10^5 cells/mL. The cells were incubated at 37℃ and 5% CO_2 incubator.

2.2. Cloning

Sequence of Lirentelimab was obtained by patent publication (PCT/US2021/071958). The heavy and light chains were cloned into pLVX recipient vector to produce lentivirus.

2.3. Lentivirus production

HEK-293T cells at a density of 1×10^6 cells per well were seeded into 6-well plates. After 24 hours, a total of 3 μg of target DNA along with lentivirus component DNA clones pMD2G and psPAX2 were co-incubated in 100 μL of PBS with polyethyleneimine (PEI) for 15 minutes. This mixture was then added to the cells. Following a 6-hour incubation period, the media was changed. After 48 hours, the cell culture media was harvested and centrifuged at 4℃ for 5 minutes at 1000 RCF. The supernatant was filtered using a 0.45 μm PES syringe filter and transferred to a tube to remove debris before being stored at -80℃.

2.4. Lirentelimab production and purification

To produce Lirentelimab, HEK-293T cells were seeded at a density of 3×10^6 cells in a 100π cultured dish. After 24 hours, 10 μg of Lirentelimab DNA was co-incubated in 200 μl of PBS with polyethyleneimine (PEI) for 15 minutes and added to the cells. Following another 24 hour incubation period, the cultured media was switched to Freestyle™ 293 Expression Medium (Invitrogen). After 120 hours, the cell culture media was harvested and centrifuged at 4℃ for 5 minutes at 1000 RCF. The resulting supernatant was stored at 4℃.

The antibody-containing culture medium was incubated with ProA™ (rProtein A Agarose Resin, Amicogen, South Korea) at 4℃ for 24 hours. Afterward, the media underwent centrifugation at 2000 RPM for 5 minutes to separate the beads. The collected beads were then transferred to a prepared activated column and washed three times with cold PBS. The antibodies were eluted from the beads using an elution buffer (75 μl of 0.1 M Citric acid solution), followed by neutralization with 25 μl of 1 M Tris in tubes. The eluted antibodies underwent dialysis twice in PBS for 6 hours

each and were subsequently concentrated using Amicon® Ultra-15 Centrifugal Filter Units (Merk, Darmstadt, Germany). The total protein content was quantified using a NanoDropTM lite Spectrophotometer.

2.5. Nanobody screening

2.5.1. Ribosome display

Ribosomal display offers the advantage of presenting approximately 10^{12} distinct library members with minimal effort. However, its widespread application has been limited due to various factors, including challenges related to reagents and unfavorable RNase activity. To overcome these technical obstacles, the in vitro translation kit PUREfrex2.1 (GeneFrontier, PF213-0.25_EX) was utilized. This kit lacks oxidized glutathione (GSSG) and the disulfide bridge isomerase DsbC, which were additionally supplemented to facilitate disulfide bond folding. Approximately 70 ng of the RNA library (equivalent to approximately 1.6×10^{12} molecules) was used as input, following the experimental protocol provided by the manufacturer. The in vitro translation reaction proceeded at 37°C for 1 hour to form ribosomal complexes.

2.5.2. *In-vitro* transcription

Both the 5’ and 3’ regions of the CDR3-randomized convex library need to be flanked prior to transcription. The 5’ flanking region and the 3’ flanking region were amplified from the plasmid pRDV5 containing Sb-convex (Addgene, 132696), using the 5’_flank_for & 5’_flank_rev primers and the 3’_flank_for & tolAK_rev primers, respectively. These flanking regions were then restricted with BspQI and ligated to each end of the library. Subsequently, the library with flanking regions

was transcribed using the T7 Ribomax ™ RNA production system (Promega, P1320) following the manufacturer's instructions.

2.5.3. Reverse transcription

The eluted RNA obtained from the Ribosomal display was subjected to reverse transcription using SuperiorScript III reverse transcriptase (Enzynomics, RT006M) with a final volume of 30 µl, following the manufacturer's instructions. The resulting cDNA was then purified using a PCR purification mini kit (Favorgen, FAGCK 001-1) with an elution volume of 30 µl. A 1 µl aliquot of the resulting eluate was utilized as a template for qPCR analysis, while the other 29 µl was reserved for PCR. The purified cDNA obtained from DNA purification was amplified via PCR using Long_FX_for and Long_Fx_rev primers, with a total reaction volume of 100 µl, which was subsequently divided into two tubes for further processing.

2.5.4. Quantitative PCR (qPCR)

Quantitative PCR (qPCR) analysis was employed to evaluate the quality of the cDNA obtained from both ribosomal display and phage display selections, enabling the monitoring of library enrichment throughout the selection process. The experiments were conducted using a QuantStudio 3 Real-time PCR instrument (Applied Biosystems) and AccuPower® 2× Greenstar qPCR master mix (Bioneer, K-6251). The PCR program conditions included an initial denaturation step at 95℃ for 2 minutes, followed by denaturation at 95℃ for 10 seconds and annealing/elongation at 63℃ for 30 seconds, with measurements taken during each cycle. The melt curve analysis was performed according to the default settings outlined in the instrument's manual.

2.5.5. Electroporation

The enriched nanobody library was incorporated into the phagemid vector pDXinit (Addgene, 110101) using FX cloning. *E. coli* SS320 cells (Lucigen, 60512-1) were thawed on ice, and a ligation mix containing the enriched library was combined with 50 µl of SS320 in an electroporation cuvette (Bio-Rad, 1652086). The cell mixture was gently pipetted and pulsed using the Bio-Rad Gene Pulser II electroporation system at 2.4 kV, 25 µF, and 300 Ω. Subsequently, the electroporated cells were promptly transferred to 25 ml of SOC medium and cultured at 37℃ with agitation at 160 rpm for 30 minutes. The recovery culture was then inoculated into 225 ml of 2YT medium supplemented with 200 µg/ml ampicillin and appropriate glucose concentration, followed by overnight incubation at 37℃ with agitation at 160 rpm.

2.5.6. Production and purification of the phage

1 ml of electroporated preculture was inoculated into 50 ml of 2YT medium supplemented with 200 µg/ml ampicillin and 2% glucose, followed by incubation at 37℃ with agitation at 160 rpm until the optical density at 600 nm (OD_{600}) reached 0.6. Subsequently, 10 ml of the culture was combined with 30 µl of M13KO7 helper phage (NEB, N0315S) and incubated at 37℃ without agitation for 1 hour. After the incubation period, the culture was centrifuged at 5,000×g for 10 minutes, and the supernatant was discarded. The pellet was resuspended in 50 ml of 2YT medium supplemented with 200 µg/ml ampicillin and 25 µg/ml kanamycin, followed by overnight incubation at 37℃ with agitation at 160 rpm.

The culture incubated overnight was then centrifuged at 6,000×g, 4℃ for 30 minutes, and 40 ml of the supernatant was transferred to a new 50 ml tube. To this, 10 ml of PEG6000/NaCl solution was added, and the tube was gently inverted. The mixture was placed on ice and incubated for 4 hours, followed by centrifugation at 10,000×g, 4℃ for 1 hour. After discarding the supernatant, the

tube was washed gently with 40 ml of PBS and subsequently resuspended in 1 ml of PBS. The resuspended phage was subsequently centrifuged at 20,000×g, 4℃ for 5 minutes, and the supernatant was transferred to a new tube. The titer of the collected phage was determined using UV-visible spectroscopy at 269 nm and 320 nm, and calculated using the equation: phages/ml = ((A269-A320) ×6 ×10^{16}) / 4900.

2.5.7. Phage display

E. coli SS320 was grown in 50 ml of 2YT medium supplemented with 10 μg/ml tetracycline, while 100 μl of 67 nM neutravidin was applied to half of a 96-well plate and incubated at 4℃ one day prior to the phage display experiment.

The neutravidin-coated plate underwent washing with 250 μl of TBS per well, followed by blocking with 250 μl of TBS-BSA (TBS with 0.5% BSA). Biotinylated Siglec-8 was combined with 4.9 ml of purified phages (at a concentration of 10^{12} phages/ml) to achieve a final protein concentration of 50 nM, then incubated on ice for 2 hours. Afterward, the neutravidin-coated plate was washed with 250 μl of TBS-BSA-D (TBS with 0.5% BSA and 0.1% tween-20). Subsequently, 100 μl of the phage-Siglec-8 mixture was added to each well of the plate and incubated on ice for one hour. Each well was washed three times with 150 μl of TBS-D (TBS with 0.1% tween-20), with the plate being dried on paper towels for 2 minutes after each wash. Following this, 100 μl of PD elution buffer (TBS supplemented with 0.25 mg/ml trypsin) was added to each well, and the plate was left to incubate at room temperature for 10 minutes. The eluted solutions were transferred to new tubes, with 40 μl of AEBSF solution (Merck, A8456) added to each tube. 1 μl of the sample was subjected to qPCR analysis, while the remaining sample was added to 50 ml of cultured SS320. This mixture was then incubated at 37℃ without shaking for 1.5 hours, followed by transfer of 50

ml of the mixture into 200 ml of 2YT medium (supplemented with 200 μg/ml ampicillin and 2% glucose), and cultured at 37℃, 160 rpm overnight.

The phages obtained from the initial round of phage display were collected and purified in TBS-BSA-D (at a concentration of 5×10^{12} phages/ml). Biotinylated Siglec-8 was introduced into 100 μl of the phage solution at a concentration of 50 nM, and the mixture was left to incubate on ice for 2 hours. Subsequently, 12 μl of Dynabeads™MyOne™Streptavidin C1 bead (Invitrogen, 65001) underwent washing with 500 μl of TBS-WTB-BSA twice, followed by blocking with 500 μl of WTB-BSA on ice for more than 20 minutes. The magnetic bead was then washed three times with 500 μl of TBS-BSA-D before being resuspended and incubated with the phage-Siglec-8 complex solution on ice for an hour. Following incubation, the mixture was washed with 500 μl of TBS-BSA-D and then resuspended in 100 μl of competition buffer, comprising TBS-BSA-D supplemented with 5 μM of non-biotinylated Siglec-8, and incubated on ice for 3 minutes. The competitive non-biotinylated Siglec-8 was subsequently removed through two washes with 500 μl of TBS-D. The bead was resuspended in 100 μl of PD elution buffer and incubated at room temperature for 10 minutes. The resulting solution was mixed by pipetting with the addition of 0.8 μl of ABESF, with 1 μl of the solution being utilized for qPCR analysis, while the rest of the solution was employed for infecting SS320. *E.coli* SS320 was cultured in 2YT media supplemented with 200 μg/ml ampicillin and 2% glucose at 37℃, 160 rpm overnight.

2.5.8. Enzyme-linked Immunosorbent Assay (ELISA)

The enriched library resulting from two rounds of phage display underwent cloning into the pSBinit vector (Addgene, 110100) using the FX cloning method. Subsequently, the cloned plasmids were introduced into *E.coli* SS320 via electroporation, followed by overnight incubation at 37℃,

160 rpm, and subsequent plasmid extraction. The extracted plasmids were subsequently transformed into *E.coli* BL21 (Enzynomics, CP110) and plated on LB-agar plates supplemented with 25 μg/ml chloramphenicol, followed by overnight incubation at 37℃.

For the preculture, 1.2 ml of TB medium supplemented with 25 μg/ml chloramphenicol was prepared in each well of a 96-well deep-well plate, labeled 'preculture'. From the incubated plate, 95 colonies were selected and inoculated into individual wells, with the first well containing the positive control, pSBinit containing the MBP nanobody Sb_MBP#1 (Addgene, 132699). The deep-well plate was then gas-permeably sealed and incubated for 4 hours at 37℃, 300 rpm.

A new 96-well deep-well plate, labeled 'expression culture', was filled with 1 ml of pre warmed TB medium supplemented with 25 μg/ml chloramphenicol. Subsequently, 50 μl of preculture was added to the corresponding well of the expression culture plate, followed by incubation at 37℃, 300 rpm for 2 hours, and then at 22℃, 300 rpm until the OD_{600} reached 0.4~0.8. Once sufficient growth was achieved, 0.02% L-(+)-arabinose was added to induce expression, followed by overnight incubation at 22℃, 150 rpm.

The following day, the cells were collected by centrifugation at 5,000×g, 4℃ for 15 minutes. The pellet from the preculture was stored at -20℃ for DNA purification, while that from the expression culture was resuspended in 100 μl of periplasmic extraction buffer (20% sucrose, 50 mM Tris, pH8.0, 0.5 mM EDTA, and 0.5 μg/ml lysozyme in DW) with vortexing. After 30 minutes of incubation on ice, 900 μl of TBS supplemented with 1 mM $MgCl_2$ was added to each well. The plate underwent centrifugation at 5,000×g, 4℃ for 15 minutes, and the supernatant was utilized as periplasmic extraction for ELISA.

Two 96-well immunoplates were coated with 100 µl of a 5 µg/ml protein A solution and left to incubate overnight at 4℃ with adhesive sealing. Following this, the plates were washed with 250 µl of TBS per well and subsequently blocked with 150 µl of TBS-BSA per well. Next, 100 µl of an anti-c-Myc antibody diluted at 1:2000 (Biolegend, 626802) in TBS-BSA-D was added to each well and incubated for 20 minutes. After three washes with 250 µl of TBS-D, 80 µl of TBS-BSA-D was added to each well, followed by the addition of 20 µl of the same periplasmic extraction, allowing for the comparison of nanobody binding between Siglec-8 and MBP. This mixture was incubated for an additional 20 minutes. Subsequently, the plates were washed three times with TBS-D, and then 100 µl of 50 nM MBP was added to the first two wells, while 100 µl of 50 nM biotinylated Siglec-8 was added to the remaining wells. The plates were then incubated for another 20 minutes. After three additional washes with TBS-D, 100 µl of a streptavidin-peroxidase solution diluted at 1:5,000 (Invitrogen, 434323) in TBS BSA-D was added to each well and incubated for 20 minutes. Following another round of washing three times with TBS-D, 100 µl of TMB substrate (Biolegend, 421101) was added to each well, and the reaction was allowed to proceed for approximately 15 minutes until the wells turned blue. Finally, the absorbance was measured at 650 nm using a plate reader.

2.6. Nanobody production and purification

A positive nanobody clone, identified through ELISA screening, was transformed into *E. coli* BL21 (DE3) cells and cultured overnight at 37°C with shaking at 160 rpm. From this overnight culture, 2 mL was inoculated into 200 mL of Terrific Broth (TB) medium containing 25 µg/mL chloramphenicol and further cultured at 37°C, 200 rpm until an optical density at 600 nm (OD_{600})

of 0.6 was reached. The temperature was then reduced to 22°C, and the culture was shaken at 150 rpm for 1 hour before the addition of 0.02% arabinose to induce protein expression. The culture was subsequently incubated overnight at 37°C, 150 rpm.

After incubation, the cells were collected by centrifugation at 5,000×g for 15 minutes at 4°C. The resulting pellet was resuspended in 20 mL of periplasmic extraction buffer and kept on ice for 30 minutes. After incubation, 180 mL of TBS buffer containing 1 mM $MgCl_2$ was added, and the solution was centrifuged at 5,000×g for 15 minutes at 4°C. The supernatant containing the nanobody was collected and divided into 50 mL aliquots.

For nanobody purification, 1 mL of TALON® Superflow™ resin (Cytiva, 28957502) was pre-equilibrated with TBS buffer (pH 8.0) and incubated with the periplasmic extract at 4°C for 1 hour with gentle rotation. After binding, the resin was washed three times with washing buffer (50 mM Tris, pH 8.0, 300 mM NaCl, and 5 mM imidazole). The nanobody was then eluted using elution buffer (50 mM Tris, pH 8.0, 300 mM NaCl, and 200 mM imidazole). The eluted nanobody was subjected to buffer exchange using a Slide-A-Lyzer® Dialysis Cassette (Thermo, 66330) overnight.

2.7. Binding assay

2.7.1. Flow cytometry based binding assay

293T cells stably expressing Siglec-8-EGFP were generated using lentiviral infection. To evaluate the binding of Siglec-8 nanobodies, cells were incubated with the nanobodies for 1 hour at room temperature. After incubation, APC-conjugated Siglec-8 antibody (BioLegend, 346007) was diluted 1:500 in PBS and added to the cells. The mixture was incubated for 30 minutes in the

dark at room temperature. Following this, the cells were washed twice with PBS to remove unbound antibody. A total of 10,000 events per sample were acquired using a BD FACSymphony flow cytometer (BD Biosciences, Franklin Lakes, NJ, USA), and the binding efficiency was analyzed with FlowJo software (BD Biosciences).

2.7.2. Bio-layer Interferometry (BLI)-based binding assay

The evaluation of nanobody binding affinity was performed utilizing the Gator Prime Instrument (Gator Bio). Streptavidin biosensors (SA) were utilized to immobilize the biotinylated antigen. The entire procedure, encompassing the establishment of baseline, antigen loading, nanobody association, and dissociation, was executed within wells of a black polypropylene 96-well microplate. To prevent nonspecific binding to the SA sensor, a reaction buffer containing 0.02% Tween-20 and 0.2% BSA was employed. The binding affinity measurement adhered to a protocol: 60 seconds for baseline establishment, followed by 120 seconds of antigen binding on the SA sensor, another 60 seconds for baseline stabilization, subsequent to which, there were 150 seconds allocated for nanobody association and 150 seconds for dissociation at 1000 rpm. The obtained binding data were fitted to a 1:1 global ligand model, and steady-state analysis was conducted to determine the binding kinetics parameters, including the dissociation constant (KD).

2.8. Reporter cell assay

2.8.1. Chimeric Siglec-8 Jurkat cell line generation

Jurkat cells stably expressing chimeric Siglec-8 and an NFAT-luciferase reporter were generated using lentiviral transduction. The chimeric Siglec-8 construct was engineered by replacing the transmembrane and intracellular domains of wild-type Siglec-8 with those of CD3 zeta. This

construct was cloned into a lentiviral vector and used to transduce Jurkat cells, followed by selection with puromycin. Similarly, NFAT-luciferase was cloned into a separate lentiviral vector, introduced into the chimeric Siglec-8-expressing Jurkat cells, and selected using blasticidin. Stable cell lines were established for use in reporter assays.

2.8.2. Luciferase assay

Jurkat cells stably expressing the chimeric Siglec-8 and NFAT-luciferase constructs were seeded at 1×10^5 cells per well in 50 µl of media in a white 96-well plate. Cells were treated with Siglec-8 nanobodies and incubated for 18 hours. After incubation, 100 µl of Bio-Glo™ Luciferase Assay Reagent (Thermo Scientific™) was added to each well, and luminescence was measured using the Varioskan™ LUX Microplate Reader (Thermo Scientific™, Waltham, MA, USA). Relative luminescence units (RLU) were recorded for each sample.

2.9. Functional assay

2.9.1. Mast cell degranulation assay

Prepare 2×10^5 of LAD2 cells stimulated either by IgE crosslinking or C48/80 stimulation alone, as well as LAD2 cells pre-incubated with nanobodies followed by IgE crosslinking or C48/80 stimulation. Rinse each cell with PBS, centrifuge, and resuspend in 50 µl of PBS. Then, dilute Pacific Blue™ anti-human CD63 antibody (Biolegend, 353011) and FITC anti-human CD107a (LAMP-1) antibody (Biolegend, 328605) at a 1:500 ratio and incubate at 4°C for 30 minutes. After washing twice with PBS, a total of 10,000 cells were counted by flow cytometry (FACSymphony, BD Biosciences, Franklin Lakes, NJ, USA) and analyzed with FlowJo software.

2.9.2 Mast cell degranulation induced drug treatments

LAD2 cells (3×10^4 per well) were treated with biotinylated IgE (200 ng/ml) for 24 hours to prime the cells for FcεRI-mediated activation. Following incubation, the cells were washed twice with HEPES secretion buffer and then treated with streptavidin (10 μg/ml) to induce FcεRI-mediated mast cell activation. Streptavidin-treated cells were incubated for 1 hour at 37°C in the absence of CO_2.

For MRGPRX2-mediated activation, LAD2 cells (3×10^4 per well) were treated with C48/80 (5 μg/ml) and incubated for 1 hour at 37°C without CO_2. Both protocols were designed to evaluate the pathways of mast cell degranulation under different activating conditions.

2.9.3. Siglec-8 clustering imaging

LAD2 cells (2×10^4 per well) stably expressing Siglec-8-EGFP were treated with Siglec-8 nanobodies and incubated for specified time intervals. Following incubation, the cells were washed once with PBS and fixed with 2% paraformaldehyde at room temperature for 15 minutes. After fixation, the cells were washed again and stained with DAPI (1 μg/ml) for nuclear visualization. Excess stain was removed with two PBS washes, and the cells were mounted onto slides using mounting media.

Confocal imaging was performed using a Carl Zeiss LSM 700 confocal microscope (Carl Zeiss AG, Oberkochen, Germany) with a 63× oil immersion objective to capture Siglec-8 clustering. Images were analyzed to evaluate clustering dynamics at different time points.

2.10. Statistical analysis

Statistical analyses were performed using GraphPad Prism 8 using unpaired student's *t* test as indicated in the figure legends. Data are presented as ± standard deviation (SD).

3. RESULTS

3.1. Screening of nanobodies with specificity for Siglec-8

To screen for nanobodies with high specificity for Siglec-8, a comprehensive screening strategy was employed, incorporating ribosome display (RD), two rounds of phage display (PD), and ELISA (Figure 1A). Ribosome display was conducted using 1.6×10^{12} mRNA strands, and qPCR analysis of the output indicated a reduction to 2.1×10^{7} mRNA strands, reflecting the initial selection pressure and enrichment.

The first round of phage display (1^{st} PD) was performed using biotinylated Siglec-8 protein immobilized on a neutravidin-coated 96-well plate. Following incubation, washing, and elution steps, qPCR analysis showed only a 0.54-fold enrichment of Siglec-8-specific binders compared to the negative control MBP, suggesting low specificity at this stage (Figure 1E).

To achieve higher specificity, the second round of phage display (2^{nd} PD) utilized biotinylated Siglec-8, which was immobilized on streptavidin-coated beads. A competitive elution strategy was implemented by introducing a high concentration of free Siglec-8 protein to displace weakly bound phages. qPCR analysis of the 2^{nd} PD output revealed a substantial 522-fold enrichment of Siglec-8-specific binders relative to MBP (Figure 1E).

The binding properties of the enriched phages were further validated using a flow cytometry assay with Siglec-8-overexpressing 293T cells. Flow cytometry histograms demonstrated a marked increase in binding for 2nd PD output phages compared to earlier rounds (Figure 1B). Quantitative analysis of GeoMean Mean fluorescence intensity (MFI) values revealed a progressive enhancement in binding efficiency across the selection process, expressed as fold changes relative to the initial input (Figure 1C).

To evaluate individual clones, 95 candidates were isolated, induced with arabinose, and tested for binding to Siglec-8 and the negative control MBP using ELISA. Clones exhibiting fold changes greater than that of the MBP nanobody (A1) were selected for further analysis (Figure 1D). Notably, while the 1st PD achieved only a 0.5-fold enrichment, the 2nd PD achieved a remarkable 455-fold enrichment compared to MBP. Of the 95 clones evaluated, 35 clones met the predefined selection criteria, and sequencing revealed 18 unique sequences (Figure 1E).

To further characterize the top candidates, the 10 highest-ranking clones from the ELISA results were expressed and analyzed via SDS-PAGE. The analysis confirmed their expression, purity, and expected molecular weight, validating their suitability for downstream studies (Figure 1F).

This systematic and iterative screening approach successfully identified Siglec-8-specific nanobodies with robust binding properties. The selected nanobody candidates represent promising tools for subsequent functional and therapeutic evaluations.

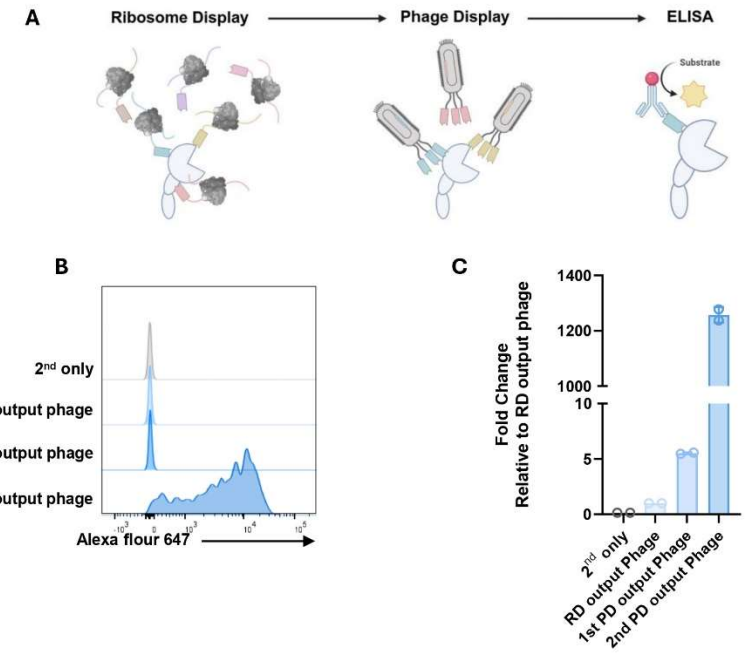

E

Nanobody selection outcome for Siglec-8	
RD input library diversity	1.6 X 10^{22}
RD output library diversity	2.1 X 10^{7}
Enrichment phage display #1	0.5 fold
Enrichment phage display #2	455.7 fold
Number of ELISA hits (out of total analyzed)	35
Number of unique sequence (out of total ELISA hits)	18
Number of expressed hits (out of unique sequence)	10*

** Top 10 selected from ELISA rankings*

F

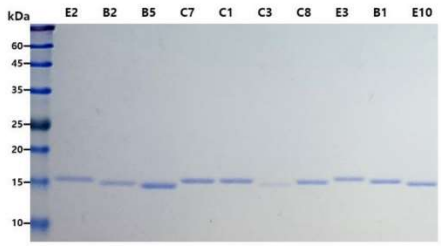

Figure 1. Screening and Enrichment of Nanobodies Targeting Siglec-8 (A) Schematic representation of the screening workflow, starting with ribosome display (RD) and followed by phage display (PD) and ELISA to identify Siglec-8-specific nanobody candidates. **(B)** Flow cytometry histograms illustrating the binding of RD, 1st PD, and 2nd PD output phages to Siglec-8-overexpressing 293T cells, demonstrating stepwise enrichment in binding specificity. **(C)** Quantification of flow cytometry results, represented as fold changes in GeoMean MFI values, confirming increased binding efficiency with each subsequent screening step. **(D)** ELISA results of 95 nanobody hits, with fold changes relative to the MBP nanobody control. Hits showing significantly higher fold changes are highlighted in blue. **(E)** Summary table of Siglec-8 nanobody screening results, providing key metrics for each selected nanobody candidate. **(F)** SDS-PAGE gel analysis of the final selected nanobody hits, confirming their purity and molecular weight.

3.2. Siglec-8 nanobodies exhibit distinct binding domains and epitope specificities

To characterize the binding specificity and structural diversity of Siglec-8-targeted nanobodies, a combination of flow cytometry, domain mapping, epitope binning, and binding kinetics measurements was employed. These analyses were designed to identify nanobodies with high specificity, diverse binding properties, and distinct structural interactions, which are critical parameters for their therapeutic potential.

The initial screening of nanobodies was conducted using recombinant purified Siglec-8 protein to identify candidates through ELISA-based methods. To further validate their binding specificity and efficacy under more physiologically relevant conditions, the top 10 nanobodies from the initial screening were evaluated for binding to Siglec-8-overexpressing 293T cells. This step aimed to refine the selection by assessing their performance in a cellular context. Flow cytometry was employed to measure binding intensity, and the 5 nanobodies with the highest GeoMean Fluorescence Intensity values were selected for subsequent analysis (Figure 2A). This approach ensured that the selected nanobodies were effective both in recombinant protein-based and cell-based assays. To further assess the binding properties of these nanobodies, EC_{50} values were determined for monomeric, dimeric, and Fc-fusion formats. Monomeric nanobodies exhibited EC_{50} values ranging from 275.42 nM to 979.49 nM, while dimeric constructs demonstrated improved binding efficiency, with EC_{50} values ranging from 19.68 nM to 221.82 nM. Among Fc-fusion constructs, the E2 Fc nanobody exhibited the highest potency, achieving an EC_{50} of 15.60 nM, which was comparable to the monoclonal antibody AK002 (3.15 nM) (Figure 2B-D; Table 1). These results

demonstrate that the dimeric format enhances binding affinity compared to the monomeric form, while the Fc-fusion format further improves potency, likely due to the multivalent binding effect.

Siglec-8, as a member of the CD33-related family of Siglecs, shares significant sequence homology with Siglec-7 and Siglec-9[33,34]. This sequence similarity necessitated the evaluation of nanobody specificity to avoid potential off-target effects. Flow cytometry analysis demonstrated that all nanobody candidates bound specifically to Siglec-8-expressing 293T cells, with no detectable binding to Siglec-7 or Siglec-9, confirming their selective targeting of Siglec-8 (Figure 2E). This high specificity supports their further development as Siglec-8-targeted therapeutics.

Domain mapping experiments were performed to elucidate the structural basis of nanobody binding and to determine whether the nanobodies targeted the V-set domain (Domain 1, D-I) of Siglec-8, known to bind its endogenous ligand 6's Lewis X and the monoclonal antibody Lirentelimab (AK002), or alternative domains. Truncation constructs representing various regions of Siglec-8 (D-I+D-II+D-III, D-I+D-II, D-I+D-III, and D-I-only) were generated and used to assess nanobody binding profiles (Figure 2F). AK002 was included as a positive control due to its well-established binding to D-I. As expected, AK002 bound to all truncated constructs, D-I+D-II+D-III, D-I+D-II, D-I+D-III, and D-I-only, confirming its specificity for D-I.

Among the nanobodies tested, B2, B5, and C3 displayed binding profiles identical to AK002, exhibiting binding to all truncated constructs. This result strongly indicates that these nanobodies specifically target D-I. In contrast, nanobodies C7 and E2 demonstrated binding to D1+D-II+D-III and D-I+D-II constructs but showed no detectable binding to D-I+D-III or D1-only constructs (Figure 2G). These results suggest that C7 and E2 specifically interact with D-II.

Biolayer interferometry (BLI) analysis was conducted to characterize the binding kinetics and affinities of the five Siglec-8-specific nanobodies, focusing on protein-protein interaction parameters (K_{on}, K_{off}, and K_D values). The results showed that dimeric formats exhibited significantly improved K_D values compared to monomeric nanobodies. Monomeric nanobodies demonstrated K_D values ranging from 79.6 nM to 960 nM, while dimeric constructs achieved values as low as 1.72 nM. This enhancement was attributed to an increase in K_{on}, indicating faster binding kinetics, while K_{off} values were higher than those of the monomeric constructs, suggesting slightly reduced stability (Figure 3A; Table 2). These findings suggest that the multivalency of the dimeric format enhances binding efficiency primarily by increasing association rates.

To further investigate whether nanobodies binding the same domain also recognized overlapping epitopes, epitope binning experiments were performed. This analysis aimed to refine the understanding of the nanobody panel's binding profiles. Among nanobodies targeting D-I, AK002 and B2 exhibited overlapping epitopes, indicating structural similarity in their binding mechanisms. Similarly, nanobodies C7 and E2, which bound to D-II, also displayed overlapping epitope specificity (Figure 3B, C). These results suggest that the nanobodies exhibit both domain-specific and epitope-specific diversity, which is critical for potential complementary therapeutic strategies.

To validate these findings and provide structural insights, docking models for the five nanobodies were generated using AlphaFold and visualized in PyMOL. The docking models aligned with experimental results, confirming specific interactions of AK002 and B2 with D-I and of C7 and E2 with D-II (Figure 3D). The structural modeling also provided detailed visualization of epitope recognition, supporting the observations from epitope binning experiments. A schematic summary

was created to integrate these findings, illustrating the diversity in binding domains and epitope specificities across the nanobody panel (Figure 3E).

The identification of nanobodies with distinct binding specificities highlights their structural diversity. While some nanobodies target the V-set domain (D-I), others exhibit preference for D-II, indicating diverse modes of interaction. This diversity provides an opportunity to leverage these nanobodies for different functional and therapeutic applications targeting Siglec-8.

These results demonstrate that the Siglec-8-specific nanobodies exhibit robust binding characteristics, domain specificity, and distinct epitope profiles. Structural and kinetic analyses confirm their selective interactions with Siglec-8, underscoring their potential for therapeutic and functional applications targeting Siglec-8.

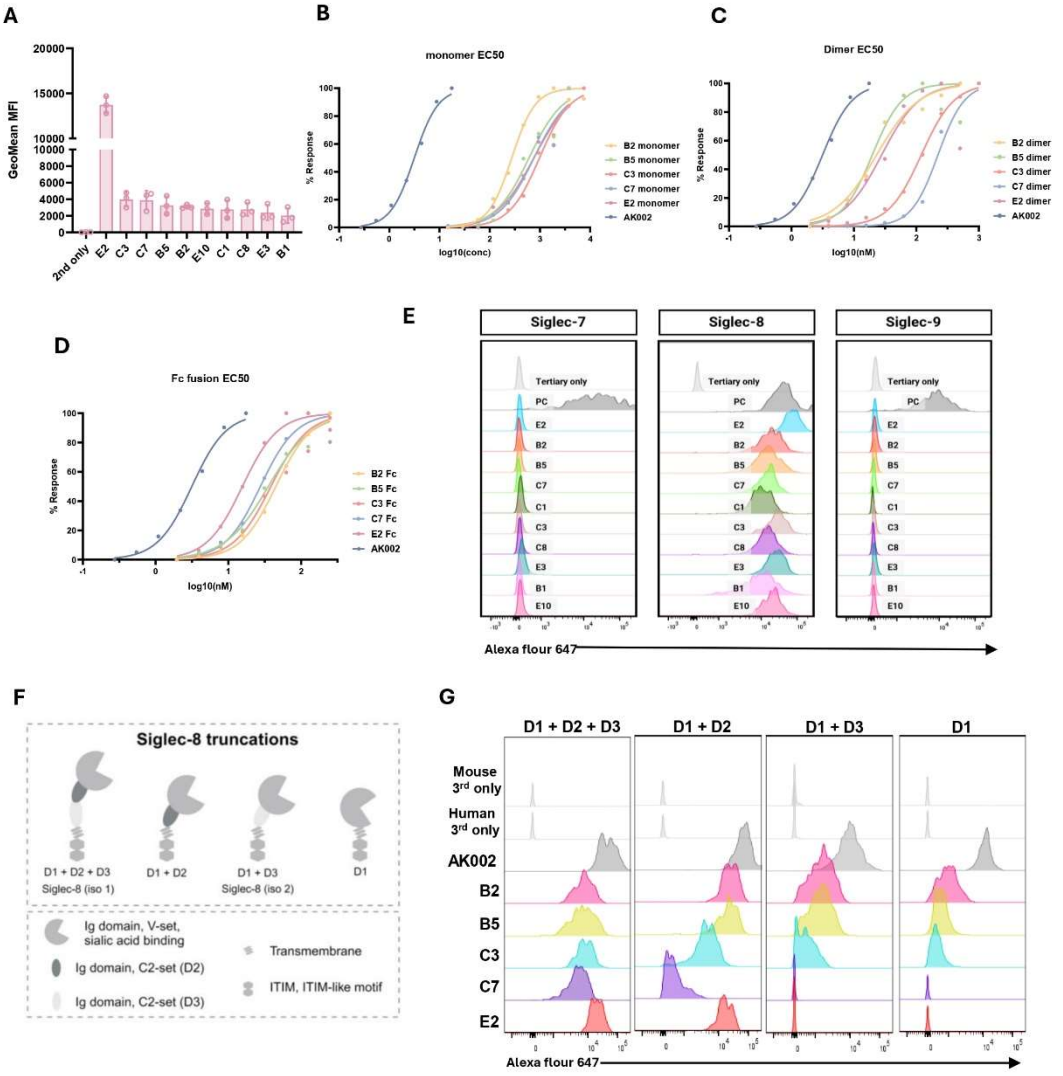

Figure 2. Binding Specificity and Epitope Mapping of Siglec-8 Nanobodies (A) Flow cytometry analysis of 10 selected nanobody candidates binding to Siglec-8-expressing 293T cells. Nanobodies were ranked based on binding intensity, and the top 5 candidates were selected for further analysis. **(B)** The EC_{50} of the nanobody monomer was determined by flow cytometry using Siglec-8-overexpressing 293T cells, providing quantitative insights into its binding efficiency. **(C)** The EC_{50} of the nanobody dimer was determined under the same conditions, demonstrating enhanced binding efficiency compared to the monomer. **(D)** The EC_{50} of the Fc-fusion nanobody was evaluated, showing distinct binding characteristics compared to the monomer and dimer formats. **(E)** Binding specificity of Siglec-8 nanobodies was assessed by flow cytometry using 293T cells transiently expressing Siglec-7, Siglec-8, or Siglec-9. All nanobodies exhibited specific binding to Siglec-8, with no cross-reactivity observed for Siglec-7 or Siglec-9. Positive controls included antibodies specific to Siglec-7, Siglec-8, and Siglec-9. **(F)** Schematic representation of Siglec-8 truncation constructs, including D-I+D-II+D-III, D-I+D-II, D-I+D-III, and D-I-only regions, to identify specific nanobody binding domains. **(G)** Binding domain analysis of the top 5 nanobodies using Siglec-8 truncation constructs, revealing specific binding patterns to distinct domains of Siglec-8.

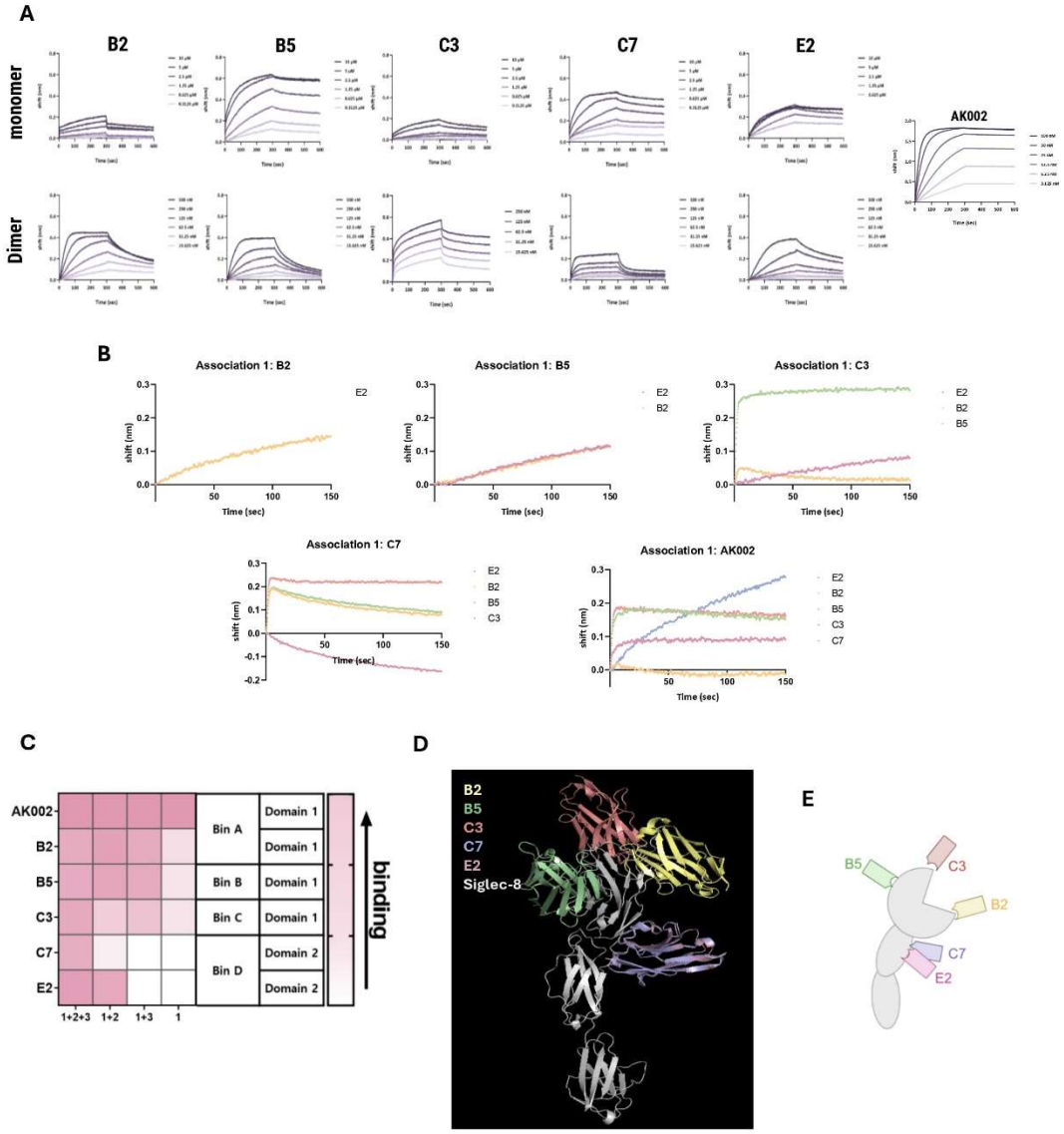

Figure 3. Comparative Affinity and Binding Analysis of Siglec-8 Nanobodies (A) Biolayer interferometry (BLI) was performed to determine the binding affinity (KD) of the reference antibody AK002, nanobody monomer, and nanobody dimer to Siglec-8. BLI analysis of nanobody monomer and dimer formats to determine their KD values, highlighting differences in binding affinity and kinetic profiles. **(B)** Epitope binning analysis of the top 5 nanobodies, demonstrating whether binding regions were distinct or overlapping. **(C)** Summary table consolidating binding domain and epitope binning results, providing a comprehensive characterization of each nanobody. **(D)** Predicted docking models of the top 5 nanobodies with Siglec-8 were generated using AlphaFold 3 and visualized with PyMOL, illustrating potential binding interactions at the structural level. **(E)** Integrated schematic summarizing epitope mapping, binding domain analysis, and docking model results, providing a holistic view of nanobody interactions with Siglec-8.

3.3. Siglec-8 nanobodies suppress mast cell activation by inducing Siglec-8 activation

To evaluate the functional effects of Siglec-8-targeted nanobodies, their ability to activate Siglec-8 and suppress mast cell degranulation was assessed using a chimeric Siglec-8 reporter system and the human mast cell line LAD2. These experiments aimed to determine whether nanobody-induced Siglec-8 activation could inhibit FcεRI- and MRGPRX2-mediated mast cell activation.

A chimeric Siglec-8 construct was engineered to facilitate quantitative measurement of activation. The wild-type Siglec-8 receptor, which contains an ITIM motif, was modified by replacing its transmembrane and intracellular domains with those of CD3 zeta, containing ITAM motifs. This construct was stably expressed in Jurkat cells, along with an NFAT-luciferase reporter system to detect calcium signaling through ITAM activation (Figure 4A). To validate the reporter system, NFAT-luciferase activity was measured following treatment with CD3/CD28 activator, which showed dose-dependent increases in relative luminescence units (RLU), confirming the functionality of the system (Figure 4B).

Next, the chimeric Siglec-8 reporter system was evaluated for Siglec-8-specific responses by treating cells with the endogenous ligand 6's Lewis X polymer. Dose-dependent increases in RLU values were observed, further demonstrating the system's responsiveness to Siglec-8 engagement (Figure 4C). To assess nanobody-induced activation, Siglec-8 nanobody monomers were tested, with AK002 (a known Siglec-8-targeting monoclonal antibody) as the positive control and an

isotype VHH (caplacizumab) as the negative control. All nanobody monomers demonstrated significant activation compared to the isotype control, although their activation levels were lower than AK002. When nanobody dimers were tested at 1 μM, significant activation was observed for all dimers relative to the isotype control, but no significant differences were detected among the dimers themselves (Figure 4D, E). These results confirm that Siglec-8-targeted nanobodies effectively activate Siglec-8.

To investigate whether Siglec-8 nanobodies could suppress mast cell activation, functional assays were performed using LAD2 cells. FcεRI-mediated activation was induced by priming cells with biotinylated IgE, followed by streptavidin treatment to induce receptor clustering. MRGPRX2-mediated activation was triggered using C48/80. Both pathways resulted in increased surface expression of degranulation markers CD63 and CD107a, with a notable increase in double-positive populations compared to unstimulated controls (Figure 5A). When the cells were treated with streptavidin in a dose-dependent manner following IgE priming, the percentage of CD63-positive cells increased proportionally, confirming successful FcεRI-mediated activation. Similarly, dose-dependent increases in the percentage of CD63-positive cells were observed following C48/80 treatment, validating the functionality of the MRGPRX2 pathway (Figure 5B, C).

To confirm that C48/80-induced activation was mediated through MRGPRX2, cells were treated with the MRGPRX2 antagonist QWF. Dose-dependent decreases in CD63 GeoMean MFI values were observed, confirming the specificity of C48/80-induced activation through MRGPRX2 (Figure 5D).

Nanobody dimers were then tested for their ability to suppress mast cell activation. When

LAD2 cells were pre-treated with nanobody dimers for 4 hours prior to FcεRI clustering, no significant inhibition of activation was observed, as indicated by similar levels of CD63 expression between nanobody-treated and untreated cells (Figure 5E). Previous studies with Siglec-8-targeting monoclonal antibodies, such as AK002, have shown that FcεRI-mediated activation in mast cells is not inhibited unless Siglec-8 and FcεRI are physically co-localized[15,35]. This co-localization was experimentally achieved by biotinylating both AK002 and anti-FcεRI antibodies, followed by neutravidin treatment to crosslink the two receptors. This receptor proximity facilitated inhibitory signaling through Siglec-8, suppressing FcεRI-mediated activation. In the absence of such co-localization, AK002 was unable to inhibit FcεRI clustering-induced activation, consistent with the inability of nanobody dimers to inhibit this pathway in the current study.

In contrast, pre-treatment with nanobody dimers for 4 hours significantly suppressed C48/80-induced activation, as evidenced by a reduction in the percentage of CD63-positive cells compared to cells treated with C48/80 alone. These results suggest that nanobody dimers effectively inhibit MRGPRX2-mediated activation via Siglec-8 engagement and its downstream signaling pathways (Figure 5F).

Collectively, these findings demonstrate that Siglec-8-targeted nanobodies can induce Siglec-8 activation and selectively suppress mast cell degranulation through the MRGPRX2 pathway. While FcεRI-mediated activation was not inhibited under the experimental conditions, previous studies with Siglec-8-targeting monoclonal antibodies, such as AK002, suggest that inhibition of FcεRI-mediated activation may be achievable with artificial co-localization of Siglec-8 and FcεRI. This possibility warrants further investigation. The strong suppression of MRGPRX2-mediated activation underscores the therapeutic potential of Siglec-8 nanobodies for targeting mast cell-

related inflammatory disorders.

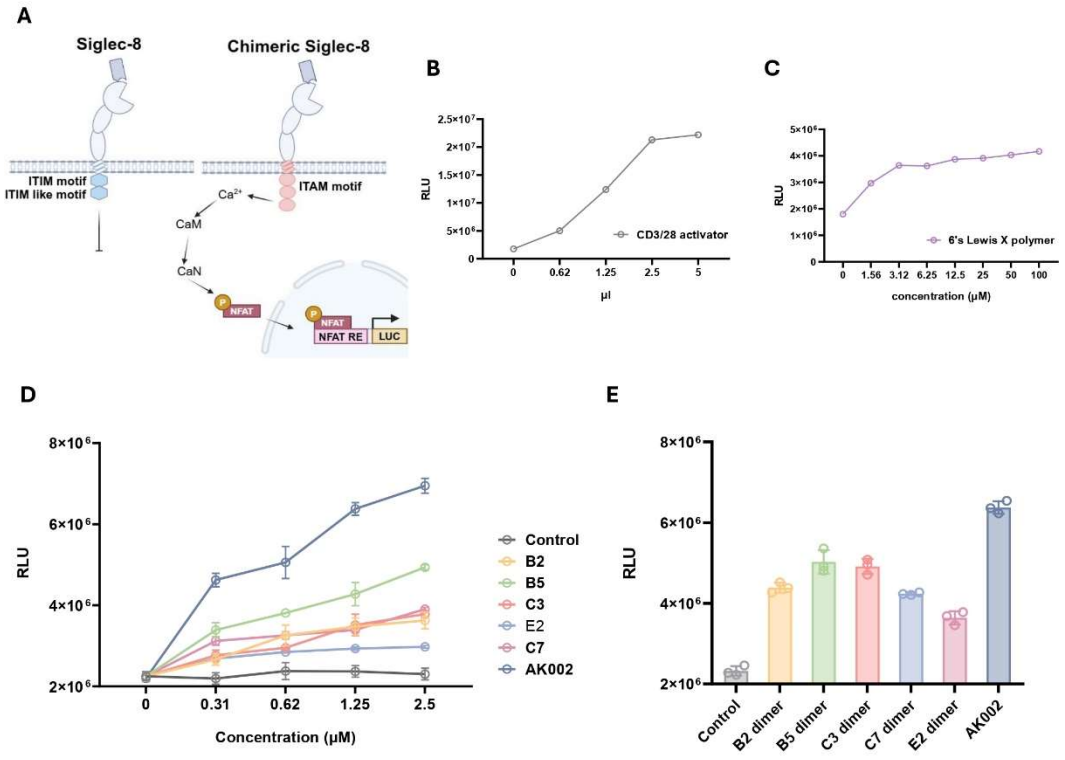

Figure 4. Evaluation of Siglec-8 Activation by Nanobodies Using a Reporter Assay (A) Schematic representation of the reporter assay system. A chimeric Siglec-8 (chSiglec-8) construct was engineered by substituting the native transmembrane and intracellular domains, including the ITIM and ITIM-like motifs, with the transmembrane and intracellular domains of CD3 zeta containing three ITAM motifs. The chSiglec-8 construct was stably expressed in Jurkat cells transduced with an NFAT-luciferase reporter system. Nanobody-mediated Siglec-8 activation was evaluated by measuring luciferase activity. **(B)** Validation of the Jurkat chSiglec-8 NFAT-luciferase cell line using CD3/CD28 activator. Increasing concentrations of the activator resulted in a dose-dependent increase in relative luminescence units (RLU), confirming successful generation and functionality of the reporter cell line. **(C)** Dose-dependent activation of the reporter cell line by 6's Lewis X polymer. The observed increase in RLU with higher concentrations of the polymer demonstrates the responsiveness and functionality of the chSiglec-8 reporter system. **(D)** Dose-

dependent activation of chSiglec-8 by nanobody monomer and AK002. Both nanobody monomer and AK002 exhibited higher activation levels compared to the Iso VHH control, confirming the functional binding of the nanobody. **(E)** Comparison of activation levels between nanobody dimer and AK002 at a fixed concentration (1 μM). While the nanobody dimer exhibited stronger activation than the Iso VHH control, its activation was lower compared to AK002.

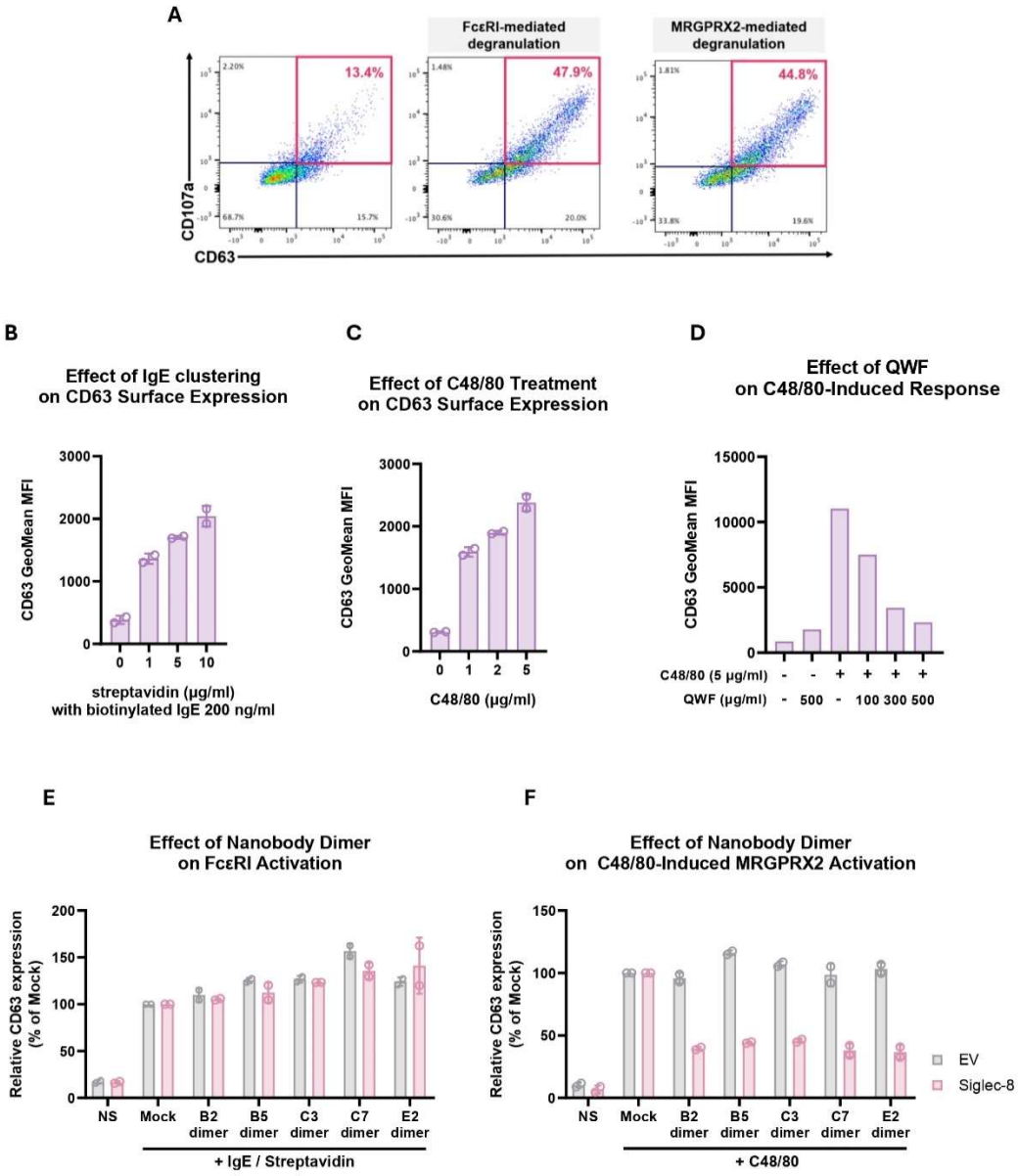

Figure 5. Inhibitory effects of Siglec-8 nanobody dimers on mast cell activation pathways (A) Mast cell activation pathways were evaluated in LAD2 cells. FcεRI-mediated activation was induced by clustering IgE-bound FcεRI receptors, while MRGPRX2-mediated activation was triggered by C48/80 treatment. Surface expression of degranulation markers CD107a and CD63 was analyzed by flow cytometry, with both pathways demonstrating increased double-positive populations compared to unstimulated controls. **(B)** FcεRI clustering-induced activation was demonstrated by treating LAD2 cells with biotinylated IgE (200 ng/ml) followed by streptavidin in a dose-dependent manner. Increased GeoMean MFI values of CD63 expression indicated successful FcεRI clustering and subsequent activation. **(C)** Dose-dependent activation of MRGPRX2 by C48/80 was confirmed by measuring CD63 expression. GeoMean MFI values increased proportionally with escalating concentrations of C48/80, validating the functionality of the MRGPRX2 signaling pathway. **(D)** The specificity of C48/80-induced activation through MRGPRX2 was confirmed using the MRGPRX2 antagonist QWF. Dose-dependent treatment with QWF significantly reduced C48/80-induced CD63 expression, verifying the role of MRGPRX2 in this pathway. **(E)** The effect of Siglec-8 nanobody dimers on FcεRI-mediated activation was assessed. While IgE stimulation resulted in increased CD63 expression, treatment with nanobody dimers did not significantly alter FcεRI-induced activation, as indicated by comparable expression levels to the stimulation control. **(F)** C48/80-induced activation via MRGPRX2 was effectively inhibited by all tested Siglec-8 nanobody dimers, as shown by reduced CD63 expression compared to the activation control. These results highlight the selective inhibitory effects of nanobody dimers on the MRGPRX2 pathway. All treatments were conducted for 4 hours prior to stimulation.

3.4. Heterodimer nanobodies induce rapid Siglec-8 clustering and inhibit mast cell activation

Previous studies have demonstrated that members of the Siglec family enhance downstream inhibitory signaling through receptor clustering[36]. For Siglec-8, while mast cell inhibition mediated by ligand-coated liposomes has been reported, no study has directly compared the inhibitory potential of receptor clustering[37]. Based on the hypothesis that clustering enhances ITIM-mediated signaling, experiments were conducted to evaluate the effect of Siglec-8 clustering on mast cell inhibition. Siglec-8 nanobody constructs containing His tags were clustered using anti-6X His antibodies, and their ability to suppress C48/80-induced MRGPRX2 activation was assessed. All five nanobody constructs showed significant inhibition upon clustering, with reductions in CD63-positive cells exceeding 10 percentage points compared to controls (Figure 6A).

To further investigate the impact of receptor clustering, heterodimer nanobody constructs were developed. Two nanobodies, B2 and C3, which share a binding domain but recognize distinct epitopes, were used to generate a B2-C3 heterodimer. This heterodimer was compared to B2 and C3 homodimers in their ability to inhibit mast cell activation. While homodimers can bind to two receptors, heterodimers have the potential to cluster multiple receptors or bind to a single receptor, depending on the context (Figure 6B).

Functional assays revealed distinct temporal differences in the inhibitory capacity of heterodimers and homodimers. At 1 hour, the B2-C3 heterodimer exhibited superior inhibition compared to either homodimer. However, at 4 hours, the C3 homodimer demonstrated greater

inhibitory capacity than the heterodimer. Additionally, while homodimers showed enhanced inhibition at 4 hours compared to 1 hour, heterodimers were more effective at 1 hour than at 4 hours (Figure 6C-E).

Confocal microscopy was used to visualize Siglec-8 clustering and internalization to understand the mechanistic basis for these observations. At both 1 hour and 4 hours, the heterodimer induced significant clustering compared to mock-treated cells. Homodimers, in contrast, exhibited stronger clustering at 4 hours compared to 1 hour (Figure 6F). Notably, heterodimers showed prominent internalization of Siglec-8 into the cytosol at 4 hours, potentially explaining their reduced inhibitory capacity at this timepoint.

These findings demonstrate that heterodimer nanobodies can rapidly induce Siglec-8 clustering, leading to effective inhibition of mast cell activation. The temporal differences in the inhibitory effects of heterodimers and homodimers suggest distinct mechanisms of action, with heterodimers providing rapid but transient inhibition, while homodimers achieve sustained inhibitory effects over longer periods. These results underscore the therapeutic potential of Siglec-8-targeted nanobody constructs and highlight the importance of receptor clustering in modulating ITIM-mediated signaling.

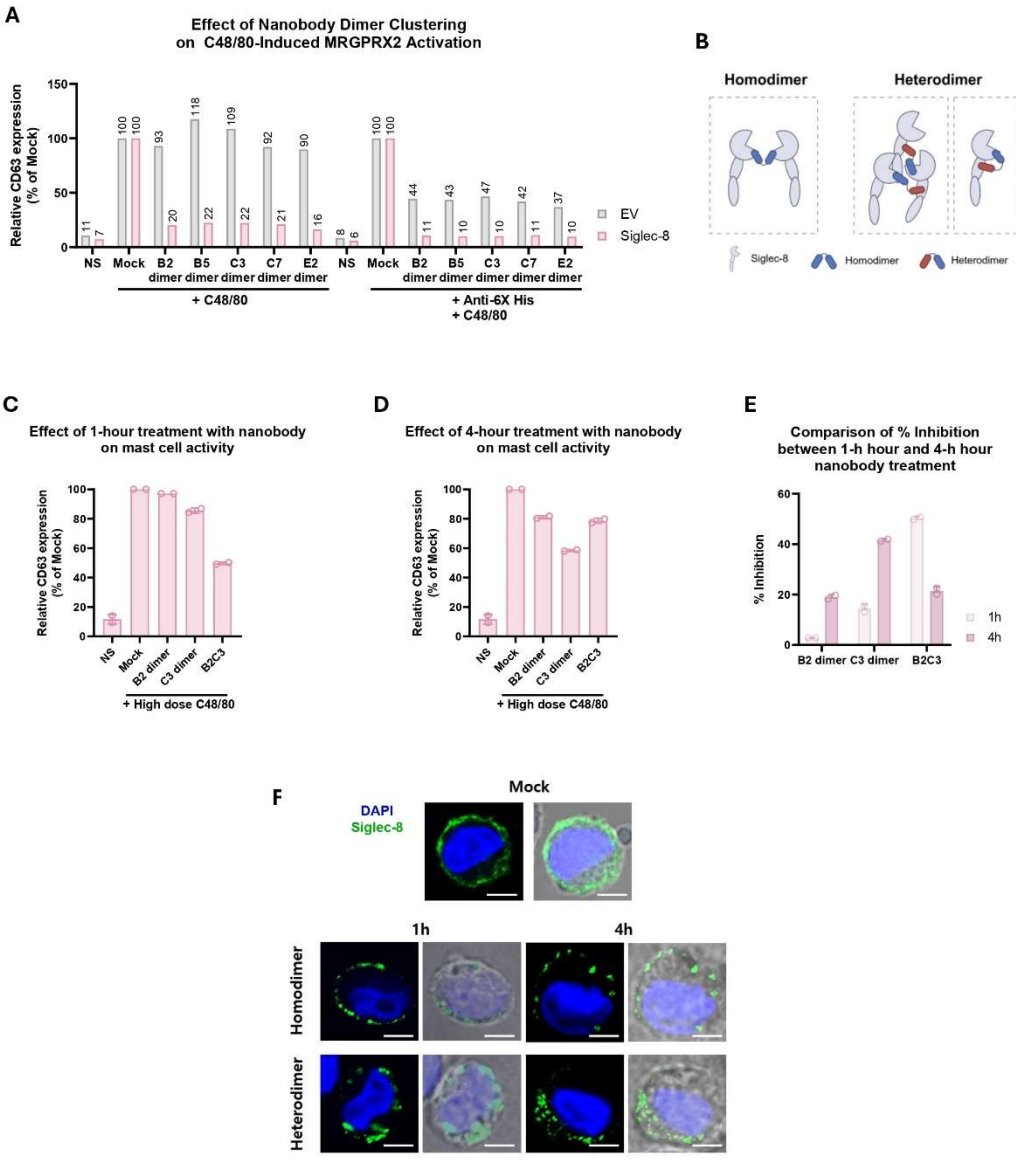

Figure 6. Comparison of Siglec-8 Nanobody Homodimers and Heterodimers in Mast Cell Inhibition and Clustering. (A) Enhanced inhibition of C48/80-induced activation was observed when Siglec-8 clustering was induced using anti-6× His antibodies targeting His-tagged nanobody dimers. Clustering resulted in significantly reduced CD63 expression in Siglec-8 overexpressing (OX) LAD2 cells compared to empty vector (EV) control cells. Partial inhibition in EV cells was attributed to the endogenous expression of Siglec-8 in LAD2 cells. **(B)** Schematic representation of homodimer and heterodimer nanobody structures. Homodimers bind exclusively to two receptors, whereas heterodimers can bind multiple Siglec-8 receptors, potentially inducing clustering. Heterodimers may also bind to a single receptor under certain conditions. **(C)** Inhibition of C48/80-induced LAD2 cell activation by nanobody homodimers and heterodimers following a 1-hour pre-incubation. Surface expression of CD63 was analyzed by flow cytometry. **(D)** Inhibition of C48/80-induced LAD2 cell activation by nanobody homodimers and heterodimers following a 4-hour pre-incubation. Surface expression of CD63 was analyzed as in (B). **(E)** Quantitative comparison of inhibition efficiencies of nanobody homodimers and heterodimers at 1-hour and 4-hour incubation times. Homodimers showed stronger inhibition at 4 hours, while heterodimers exhibited greater inhibition at 1 hour. Data are presented as the percentage of inhibition relative to untreated controls. **(F)** Immunofluorescence analysis of Siglec-8 clustering following treatment with homodimers or heterodimers for 1 hour or 4 hours. LAD2 cells stably expressing Siglec-8-EGFP were used, with Siglec-8 localization visualized by EGFP (green) and nuclei stained with DAPI (blue). Heterodimers (B2-C3 heterodimer) induced rapid clustering at 1 hour, whereas homodimers (C3 homodimer) promoted clustering more prominently at 4 hours. Scale bar represents 5 μm.

4. Discussion

This study demonstrates the potential of Siglec-8-targeted nanobodies as effective modulators of mast cell activation through receptor clustering and ITIM-mediated signaling. By systematically evaluating the binding characteristics, activation potential, and inhibitory effects of these nanobodies, we provide new insights into the mechanisms underlying Siglec-8-mediated mast cell suppression.

Our results confirm that Siglec-8 nanobodies can selectively bind to Siglec-8 with high specificity, as evidenced by the absence of cross-reactivity with closely related Siglecs such as Siglec-7 and Siglec-9[34]. The diversity in binding domains and epitope specificities among the nanobodies highlights their structural variability, which could influence their functional properties. Notably, nanobody dimers demonstrated enhanced binding affinity and functional potency compared to monomers, consistent with the avidity effect. These findings are foundational for designing optimized nanobody-based therapeutics targeting Siglec-8.

The chimeric Siglec-8 reporter assay confirmed that all nanobody constructs effectively activated Siglec-8. This was further validated by comparing their activity to AK002, a monoclonal antibody targeting Siglec-8. While the nanobody constructs exhibited lower activation levels than AK002, their functional ability to induce Siglec-8 activation was significant and consistent across monomeric and dimeric formats. This suggests that Siglec-8 nanobodies can effectively engage ITIM signaling pathways, which are critical for suppressing mast cell activity.

In mast cell functional assays, nanobody dimers exhibited strong inhibitory effects on

MRGPRX2-mediated activation, significantly reducing the surface expression of degranulation markers CD63. The observed suppression of MRGPRX2-mediated activation aligns with prior findings that Siglec-8 activation inhibits mast cell degranulation. Interestingly, FcεRI-mediated activation was not inhibited under the experimental conditions. However, previous studies with Siglec-8-targeting antibodies have demonstrated that FcεRI inhibition requires the artificial co-localization of Siglec-8 and FcεRI[15,35]. This suggests that nanobody dimers may also suppress FcεRI activation under conditions that facilitate receptor proximity, warranting further investigation.

The most striking finding of this study is the role of receptor clustering in enhancing the inhibitory effects of Siglec-8 nanobodies. By clustering Siglec-8 using anti-6X His antibodies, we observed significant improvements in mast cell inhibition. Furthermore, heterodimer nanobodies, designed to target distinct epitopes on Siglec-8, demonstrated superior inhibitory effects compared to homodimers at early time points. However, their reduced efficacy at later time points correlated with the internalization of Siglec-8 into the cytosol, as observed via confocal microscopy. In contrast, homodimers showed sustained inhibitory effects at later time points, consistent with their enhanced clustering at 4 hours. These temporal differences suggest distinct mechanisms of action between homodimers and heterodimers, with heterodimers providing rapid but transient inhibition and homodimers achieving more sustained effects.

This study provides important implications for the development of Siglec-8-based therapeutics. The ability of nanobody heterodimers to induce rapid clustering and potent inhibition makes them attractive candidates for acute inflammatory conditions where immediate suppression of mast cell activity is required. On the other hand, homodimers may be more suitable for chronic conditions due to their sustained inhibitory effects. Additionally, the observed internalization of Siglec-8 upon

heterodimer engagement raises the possibility of utilizing such constructs for receptor-mediated delivery of therapeutic agents.

While these findings highlight the therapeutic potential of Siglec-8-targeted nanobody constructs, several questions remain. For instance, the precise molecular mechanisms underlying the differences in temporal efficacy between homodimers and heterodimers require further investigation. Moreover, optimizing the delivery and stability of these constructs in vivo will be critical for their clinical translation.

In conclusion, this study establishes Siglec-8-targeted nanobodies as versatile tools for modulating mast cell activity. By elucidating the importance of receptor clustering in ITIM-mediated signaling, these findings lay the groundwork for the development of next-generation therapeutics for mast cell-mediated inflammatory disorders.

5. Conclusion

This study demonstrates that Siglec-8-targeted nanobodies effectively suppress mast cell activation through ITIM-mediated signaling, with receptor clustering playing a critical role in enhancing inhibitory effects on IgE-independent signaling of mast cells. While heterodimer nanobodies induced rapid clustering and transient inhibition, homodimers provided sustained inhibition by promoting prolonged clustering. These findings highlight the therapeutic potential of Siglec-8 nanobody for targeting mast cell-mediated inflammatory signaling and provide a foundation for developing next-generation therapies aimed at treating allergic inflammatory diseases.

References

1 Lin Y, Zhu Z, Aodeng S, Wang X, Wang L, Wang W, et al. Ambient air pollution and risk of allergic respiratory diseases in European and East Asian populations: A Mendelian randomization study. Ecotoxicol Environ Saf 2024;286:117205.
2 Hillerich V, Valbert F, Neusser S, Pfaar O, Klimek L, Sperl A, et al. Quality of life and healthcare costs of patients with allergic respiratory diseases: a cross-sectional study. Eur J Health Econ 2024;25:579-600.
3 Gupta RS, Warren CM, Smith BM, Jiang J, Blumenstock JA, Davis MM, et al. Prevalence and severity of food allergies among US adults. JAMA Netw Open 2019;2:e185630.
4 Alghamdi AS, Alwadeai KS, Almeshari MA, Alhammad SA, Alsaif SS, Alshehri WA, et al. Prevalence of obesity and its associated comorbidities in adults with asthma: a single-center study in Saudi Arabia. Medicina (Kaunas) 2024;60:1785.
5 Guntern P, Eggel A. Past, present, and future of anti-IgE biologics. Allergy 2020;75:2491-502.
6 Lin H, Boesel KM, Griffith DT, Prussin C, Foster B, Romero FA, et al. Omalizumab rapidly decreases nasal allergic response and FcepsilonRI on basophils. J Allergy Clin Immunol 2004;113:297-302.
7 Müller UR. Recent developments and future strategies for immunotherapy of insect venom allergy. Curr Opin Allergy Clin Immunol 2003;3:299-303.
8 Metz M, Kolkhir P, Altrichter S, Siebenhaar F, Levi-Schaffer F, Youngblood BA, et al. Mast cell silencing: A novel therapeutic approach for urticaria and other mast cell-mediated diseases. Allergy 2024;79:37-51.
9 Sabato V, Beyens M, Toscano A, Van Gasse A, Ebo DG. Mast cell-targeting therapies in mast cell activation syndromes. Curr Allergy Asthma Rep 2024;24:63-71.
10 Korver W, Benet Z, Wong A, Negri GL, Chang K, Sanchez R, et al. Regulation of mast cells by overlapping but distinct protein interactions of Siglec-6 and Siglec-8. Allergy 2024;79:629-642.
11 Kim YH, Park CS, Lim DH, Lee JH, Park HS, Lee MG, et al. Antiallergic effect of anti-Siglec-F through reduction of eosinophilic inflammation in murine allergic rhinitis. Am J Rhinol Allergy 2013;27:187-91.
12 Lim SYT, Huo J, Laszlo GS, Cole FM, Kehret AR, Li J, et al. Optimizing Siglec-8-directed immunotherapy for eosinophilic and mast cell disorders. Cancers (Basel) 2024;16:3476.
13 Lim SYT, Huo J, Laszlo GS, Cole FM, Kehret AR, Li J, et al. Optimizing Siglec-8-directed immunotherapy for eosinophilic and mast cell disorders. Cancers (Basel) 2024;16:3476.
14 Trindade CJ, Sun X, Maric D, Sharma S, Komarow HD, Hourigan CS, et al. Flow cytometric immunophenotypic differentiation patterns of bone marrow eosinophilopoiesis. Cytometry B Clin Cytom 2024;106:370-82.
15 Korver W, Wong A, Gebremeskel S, Negri GL, Schanin J, Chang K, et al. The inhibitory receptor Siglec-8 interacts with FcεRI and globally inhibits intracellular signaling in primary mast cells upon activation. Front Immunol 2022;13:833728.
16 Treudler R, Simon JC. Developments and perspectives in allergology. J Dtsch Dermatol Ges 2023;21:399-403.
17 O'Sullivan JA, Youngblood BA, Schleimer RP, Bochner BS. Siglecs as potential targets of therapy in human mast cell- and/or eosinophil-associated diseases. Semin Immunol

2023;69:101799.
18 Castells M, Madden M, Oskeritzian CA. Mast cells and Mas-related G protein-coupled receptor X2: itching for novel pathophysiological insights to clinical relevance. Curr Allergy Asthma Rep 2025;25:5.
19 Chow TG, Muzaffar AF, Alvarez-Arango S. Non-IgE-mediated drug-induced hypersensitivity reactions in pediatrics. Curr Opin Pediatr 2024;36:674-83.
20 He X, Yang X, Qin L, Zhang Q, Ji X, Tang W, et al. Amphotericin B for injection triggers degranulation of human LAD2 mast cells by MRGPRX2 and pseudo-allergic reactions in mice via MRGPRB2 activation. Immunol Res 2024;72:1337-49.
21 West PW, Chéret J, Bahri R, Kiss O, Wu Z, Macphee CH, et al. The MRGPRX2-substance P pathway regulates mast cell migration. iScience 2024;27:110984.
22 Bawazir M, Sutradhar S, Roy S, Ali H. MRGPRX2 facilitates IgE-mediated systemic anaphylaxis in a newly established knock-in mouse model. J Allergy Clin Immunol 2024;in press.
23 Wollam J, Solomon M, Villescaz C, Lanier M, Evans S, Bacon C, et al. Inhibition of mast cell degranulation by novel small molecule MRGPRX2 antagonists. J Allergy Clin Immunol 2024;154:1033-43.
24 Johal KJ, Saini SS. Current and emerging treatments for chronic spontaneous urticaria. Ann Allergy Asthma Immunol 2020;125:380-7.
25 Robinson WH, Moreland L, Deodhar M, Harler MB, Saulsbery C, Kunder R. Cutting-edge approaches to B-cell depletion in autoimmune diseases. Front Immunol 2024;15:1454747.
26 Hiemstra IH, Santegoets KCM, Janmaat ML, de Goeij BECG, ten Hagen W, van Dooremalen S, et al. Preclinical anti-tumour activity of HexaBody-CD38, a next-generation CD38 antibody with superior complement-dependent cytotoxic activity. EBioMedicine 2023;93:104663.
27 Gorska MM. Update on Type 2 Immunity. J Allergy Clin Immunol 2024;in press.
28 Niehues T, von Hardenberg S, Velleuer E. Rapid identification of primary atopic disorders (PAD) by a clinical landmark-guided, upfront use of genomic sequencing. Allergol Select 2024;8:304-23.
29 Dellon ES, Peterson KA, Murray JA, Falk GW, Gonsalves N, Chehade M, et al. Anti-Siglec-8 antibody for eosinophilic gastritis and duodenitis. N Engl J Med 2020;383:1624-34.
30 Yang EY, Shah K. Nanobodies: Next generation of cancer diagnostics and therapeutics. Front Oncol 2020;10:1182.
31 Shen Z, Sang Z, Shi Y. Nanobodies as a powerful platform for biomedicine. Trends Mol Med 2022;28:1006-7.
32 Zimmermann I, Egloff P, Hutter CAJ, Kuhn BT, Bräuer P, Newstead S, et al. Generation of synthetic nanobodies against delicate proteins. Nat Protoc 2020;15:1707-41.
33 Siddiqui SS, Matar R, Merheb M, Hodeify R, Vazhappilly CG, Marton J, et al. Siglecs in brain function and neurological disorders. Cells 2019;8:1125.
34 Crocker PR, Paulson JC, Varki A. Siglecs and their roles in the immune system. Nat Rev Immunol 2007;7:255-66.
35 Duan S, Xia Y, Zaia J, He X, Shi P. Nanoparticles displaying allergen and Siglec-8 ligands suppress IgE-FcεRI-mediated anaphylaxis and desensitize mast cells to subsequent antigen challenge. J Immunol 2021;206:2290-300.
36 Conti G, Bärenwaldt A, Rabbani S, Mühlethaler T, Sarcevic M, Jiang X, Schwardt O, Ricklin D, Pieters RJ, Läubli H, Ernst B. Tetra- and hexavalent Siglec-8 ligands modulate

immune cell activation. Angew Chem Int Ed Engl 2023;62:e202314280.
37 Lenza MP, Bärenwaldt A, Ambrosi M, Rademacher C, Reichardt NC, García-Fernández JM, et al. Structures of the inhibitory receptor Siglec-8 in complex with a high-affinity sialoside analogue and a therapeutic antibody. JACS Au 2023;3:204-15.

APPENDICES

Table 1. EC_{50} values of nanobody monomers, dimers, and Fc-fusion constructs for Siglec-8 binding

EC_{50} (nM)	B2	B5	C3	C7	E2	AK002
Monomer	275.42	606.74	979.49	762.08	756.83	
Dimer	23.01	19.68	119.95	221.82	27.80	3.15
Fc-fusion	44.98	35.48	38.55	27.61	15.60	

Table 2. Biolayer Interferometry (BLI) analysis of binding kinetics for nanobody monomers and dimers

	Monomer				Dimer			
	Koff (1/s)	Kon (1/Ms)	KD(M)		Koff (1/s)	Kon (1/Ms)	KD(M)	
AK002	4.76E-5	3.58E+5	1.33E-10	133 pM				
B2	2.34E-3	3.50E+3	6.69E-7	669 nM	2.73E-3	5.52E+4	4.95E-8	49.5 nM
B5	3.04E-4	3.82E+3	7.96E-8	79.6 nM	5.56E-3	3.66E+4	1.52E-7	152 nM
C3	1.39E-3	1.45E+3	9.60E-7	960 nM	1.07E-3	6.21E+5	1.72E-9	1.72 nM
E2	6.48E-4	1.30E+3	4.98E-7	498 nM	2.02E-3	1.50E+4	1.35E-7	135 nM
C7	6.09E-4	2.97E+3	2.05E-7	205 nM	9.67E-3	9.96E+4	9.71E-8	97.1 nM

Abstract in Korean

Siglec-8을 타겟하는 신규 나노바디를 활용한 비만세포의 활성 조절

비만세포(Mast cell)는 알레르기 염증에서 중요한 역할을 담당하며, 천식과 만성 두드러기와 같은 질환에서 주요한 치료 표적으로 여겨지고 있습니다. Siglec-8은 비만세포와 호산구에만 선택적으로 발현되는 억제 수용체로, ITIM(면역수용체 티로신 기반 억제 모티프)을 매개한 신호 전달을 통해 비만세포와 호산구의 활성화를 억제할 수 있는 능력으로 주목받고 있습니다. 본 연구에서는 Siglec-8에 특이적으로 결합하는 나노바디(nanobody)를 개발하고, 각각의 결합 특성을 가지는 동질이량체 (homodimer) 및 이질이량체 (heterodimer) 형식을 포함한 다양한 나노바디를 특성화하였습니다.

본 연구 결과, 이질이량체 나노바디는 Siglec-8의 클러스터링(clustering)을 빠르게 유도하여 처리 후 1시간 이내에 비만세포 활성화를 효과적으로 억제하는 것으로 나타났습니다. 이와 달리 동질이량체 나노바디는 상대적으로 느리지만 지속적인 억제 효과를 보였으며, 이는 세포 표면에서 Siglec-8의 장기간 클러스터링과 관련이 있음을 확인하였습니다. 이러한 결과는 Siglec-8 나노바디 변이체가 시간적 및 기능적

메커니즘에서 차별적인 특성을 가지고 있음을 시사합니다.

본 연구는 Siglec-8 클러스터링을 통한 비만세포 활성 억제의 가능성을 제시하며, 알레르기 및 염증성 질환을 치료하기 위한 표적화되고 안전한 치료법 개발의 기초를 제공합니다.

핵심되는 말: 비만세포, 알레르기 염증, Siglec-8, 나노바디, ITIM 모티프, 억제성 수용체, 수용체 클러스터링